The Molecular Composition of Square Arrays†

Jan Gunnar Sorbo, Svein Erik Moe, Ole Petter Ottersen, and Torgeir Holen*

Center for Molecular Biology and Neuroscience (CMBN), and Nordic Center of Excellence for Research in Water Imbalance Related Disorders (WIRED), University of Oslo, Oslo 0317, Norway

Received October 25, 2007; Revised Manuscript Received December 18, 2007

ABSTRACT: Square arrays are prominent structures in plasma membranes of brain, muscle, and kidneys with an unknown function. So far, the analysis of these arrays has been restricted to freeze fracture preparations, which have shown square arrays to contain the water channel Aquaporin-4 (AQP4). Using Blue-Native PAGE immunoblots, we provide evidence that higher-order AQP4 complexes correspond to square arrays, with the AQP4 isoform M23 playing a dominant role. Our data are consistent with the idea that square arrays consist of aggregates of AQP4 tetramers complexed with multiples of dimers. By comparison, Aquaporin-1 and Aquaporin-9 form tetramers, but not higher-order complexes. AQP4 square arrays are stable under several biochemical purification steps. Analyzing the internal composition of the higher-order complexes by 2D gels, we demonstrate that the square arrays in addition to M23 also invariably contain AQP4, M1, and a novel AQP4 isoform that we call Mz. The visualization AQP4 square arrays by a rapid, biochemical assay provides new insight in the molecular organization of square arrays and gives further proof of the heterogeneity of AQP4 square arrays in vivo.

Well-ordered, square arrays of intramembrane particles (IMP),[1] which are also called orthogonal arrays of proteins (OAPs), were first discovered by freeze-fracture electron microscopy more than 30 years ago (*1*−*5*). These arrays are impressive structures—often containing several hundred IMPs—and show a great diversity of size, shape, and substructure. The physiological role of square arrays has remained enigmatic. In the membranes of the lens of the eye, Aquaporin-0 (AQP0) constitutes one form of square array, which has been extensively analyzed (*6*−*9*). In the brain, kidneys, and muscle, there is strong evidence that Aquaporin-4 (AQP4) is a main component of square arrays (*10*), because the square arrays disappear in AQP4 knockout mice (*11*) and have been directly observed to contain AQP4 by freeze-fracture replica immunogold labeling (FRIL) electron microscopy (*12*). Furthermore, mice that overexpress AQP4 exhibit a higher density of square arrays than wild type mice (*13*). In the brain, square arrays are most densely concentrated in astrocyte endfeet membranes (*2*, *12*).

AQP4 is the aquaporin most strongly expressed in the brain (*14*). Consistent with the idea that AQP4 is a main constituent of square arrays, this water channel is very abundant in astrocytic endfeet membranes in contact with blood vessels and pia. AQP4 is also present in ependymal cells lining the ventricles, and in glial lamellae in the supraoptic nucleus and other circumventricular organs (*15*). This pattern of expression suggests that AQP4 is involved in transport of water at the brain/blood and brain/CSF interfaces and also indicates a role in osmotransduction (*14*, *15*). In agreement, studies of AQP4 −/− mice and mice with a disruption of AQP4 anchoring (mdx and alpha-syntrophin−/− mice) have implicated AQP4 in a long list of physiological and pathophysiological processes (*16*, *17*). The most striking effect of AQP4 knock-out is reduced brain edema after acute water intoxication and ischemic stroke (*18*). Recently, AQP4 was proposed to serve a role as an adhesion molecule in cell−cell interactions (*6*).

AQP4 is known to have two major isoforms (M1 and M23), and the atomic structure of the purified and reconstituted latter isoform was recently published (*6*). Upon transfection into the CHO cell line, the M23 isoform has been demonstrated by freeze-fracture electron microscopy to give rise to structures reminiscent of square arrays (*12*, *19*). It has been proposed that the ratio of the two isoforms M1 and M23 is central in the regulation of square array structures, and thus possibly in the regulation of water transport (*20*, *21*).

Here, we provide the first analysis of square arrays by a technique other than freeze-fracture electron microscopy. Using Blue-Native PAGE (BN-PAGE), combined with immunoblotting, we show that AQP4 forms tetramers and higher-order protein complexes in tissues from rat brain and rat nasal mucosa, and in transfected HeLa cells. By comparison, AQP1, another brain aquaporin, and AQP9, which is a liver aquaporin, do form tetramers, but not higher-order complexes. We show that the main higher-order complexes of AQP4 have the same apparent molecular weight in mouse brain and M23 transfected HeLa cells as they do in rat tissue.

* Author to whom correspondence should be addressed. Tel.: +47 22 85 12 94. Fax: +47 22 85 14 88. E-mail: torgeir.holen@medisin.uio.no.

† Funding information: J.G.S. and S.E.M. have grants from Forskerlinjen, the Medical Student Research Programme at the University of Oslo. T.H. has a grant from The Norwegian Cancer Society. This work was supported by the Nordic Centre of Excellence Program in Molecular Medicine and the Research Council of Norway (Storforsk Program), and FUGE (Norwegian Functional Genomics Program).

[1] Abbreviations: AQP4, aquaporin-4; AQP1, aquaporin-1; AQP9, aquaporin-9; AQP0, aquaporin-0; BN-PAGE, blue native−polyacrylamide gel electrophoresis; IMP, intramembrane particles; FRIL, freeze-fracture replica immunogold labeling; OAP, orthogonal arrays of proteins; CSF, cerebrospinal fluid; mdx, mice lacking dystrophin; DDM, dodecyl-β-D-maltoside.

10.1021/bi702146k CCC: $40.75
Published on Web 02/02/2008

The square arrays are stable under several biochemical purification steps, then gradually break down to the component monomers, dimers, and trimers. By combining BN-PAGE with second-dimension (2D) SDS-PAGE, we analyze the composition of the square arrays, showing them to contain the dominant isoform M23, in addition to the isoform M1 and a third isoform, Mz. The introduction of a rapid biochemical assay to complement the technically challenging and time-consuming freeze-fracture technique gives new insight in the molecular organization of square arrays.

EXPERIMENTAL PROCEDURES

Lysate Preparation for Blue-Native PAGE (BN-PAGE). Male adult PVG rats were sacrificed by elevated CO_2 and decapitated. The brain was dissected and homogenized in chilled 50 mM HEPES pH 7.4, 2 mM EDTA, 0.32 M sucrose, and protease inhibitor cocktail (PIC, Roche), then centrifuged 1000 g for 10 min, yielding the P1 (nuclear pellet) and S1 (post-nuclear supernatant) fractions. S1 was subjected to another round of centrifugation at 164 000 g for 30 min using a Beckman Ti70 rotor. The resulting supernatant S2 (cytosolic fraction) was decanted, and the pellet P2 constituted the crude membrane fraction. P2 was resuspended in 50 mM HEPES pH 7.4, 2 mM EDTA, and PIC and stored at −20 °C. Mouse brain and rat liver was prepared in the same manner. For rat nasal mucosa samples, the S1 fraction was used directly. Transfected cells lysates were prepared by lysing the cells in the well with 1X NativePAGE sample buffer supplemented with 1% w/v dodecyl-β-D-maltoside (DDM, Sigma) for 15 min at room temperature. The lysate was pipetted off, sonicated, and centrifuged at 23 000 *g* for 10 min; then, the pellet was discarded. The supernatant was concentrated using 10-kDa cutoff spin columns (PALL).

Lysate Preparation for SDS-PAGE. Cell lysates were made as previously described, except that the lysis buffer was 1% sodium dodecyl sulfate (SDS), 10 mM sodium phosphate pH 7.4, 150 mM NaCl, 5 mM EDTA, and PIC. Brain tissue was homogenized directly in the same lysis buffer, sonicated, centrifuged at 23 000 *g* for 10 min and pellet discarded. The total protein in all samples was determined using the DC-total protein kit (Bio-Rad).

BN-PAGE. Lysates were diluted with NativePAGE Sample Buffer (Invitrogen) supplemented with 0.5−1% w/v DDM, incubated 15 min at room temperature, and centrifuged at 23 000 *g* for 10 min; then, the pellet was discarded. All samples were adjusted to a final Coomassie G-250:detergent-ratio of 1:4 immediately prior to gel loading. NativeMARK (Invitrogen LC0725) was used as a molecular weight marker.

Electrophoresis was performed at room temperature. The gels used were 3%−12% NativePAGE (Invitrogen) and were run in one-third of the migration at 150 V with the dark cathode buffer (Invitrogen) and at 150 V with the light cathode buffer (Invitrogen) until the dye reached the gel bottom. Control experiments were conducted with 4%−16% NativePAGE gels to validate the molecular weight estimates. Gels were blotted onto PVDF, according to the manufacturer's instructions (Invitrogen). Blots were extensively destained with methanol, stained with PonceauS to visualize and label the molecular weight marker, and finally destained with 0.1 M NaOH. Blocking and immunodetection were performed as described for SDS-PAGE blots.

Cell Culture and Plasmid Transfections. HeLa cells were maintained in DMEM supplemented with 1% L-glutamine (Cambrex) and 10% foetal calf serum (Gibco BRL). The cells were passaged at sub-confluency and transfected with plasmids using 200 μL OptiMem (Gibco), FuGENE6 (Roche) at a 3:1 ratio (μL:μg nucleic acid), and 0.17 μg of DNA per square centimeter. The medium was changed after 4 h. Cells were harvested 24 h after transfection. The M1 and M23 plasmids were prepared by Endotoxin-free MaxiPreps (Qiagen).

SDS-PAGE/Immunoblotting. SDS-PAGE and immunoblotting has been optimized, with respect to AQP4 resolution (*22*). Briefly, gels were composed of 12% Laemmli PAGE supplemented with 3 M urea and the loading buffer was 1.7% SDS, 60 mM Tris pH 6.8, 5% glycerol, 100 mM DTT, and trace amounts of bromophenol blue. Samples were not heated prior to loading. MagicMarkXP (Invitrogen LC5602) was used as a molecular weight marker. Proteins were blotted onto PVDF membranes that were blocked with 5% milk powder and incubated with primary antibody diluted in the blocking solution overnight at 4 °C and detected with the ECF kit, according to the manufacturer's instructions (Amersham).

Purification of AQP4. AQP4 was purified from male Wistar brain and verified by matrix-assisted laser-desorption ionization-time-of-flight mass spectroscopy (MALDI-TOF MS) (Sorbo et al., unpublished). Briefly, purification included plasma membrane isolation, membrane stripping, detergent solubilization, and several chromatographic steps. Aliquots from each step were analyzed by BN-PAGE as described previously.

2D BN-PAGE/SDS-PAGE. Twenty micrograms (20 μg) of rat brain membranes were separated by 3%−12% BN-PAGE, as described previously. After electrophoresis, the lane was cut out from the gel and equilibrated in a SDS-loading buffer supplemented with 100 mM DTT for 15 min at room temperature. The lane was then loaded into an IPG well on a 12% Laemmli gel supplemented with 3 M urea. The well was overlaid with 0.5% agarose suspended in Laemmli buffer and allowed to solidify. SDS-PAGE and immunoblotting were then performed as described previously.

Antibodies. Rabbit-anti-AQP4 (Chemicon AB3068) and rabbit-anti-AQP1 (Alpha Diagnostics AQP1-1A) were used at a final concentration of 1 μg/mL, whereas rabbit-anti-AQP9 (Alpha Diagnostics AQP9-1A) were used at a final concentration of 10 μg/mL.

RESULTS AND DISCUSSION

Optimization of BN-PAGE Detergents. We have previously optimized the conditions for the denaturing gel electrophoresis analysis of AQP4 (*22*). To address the native conformation of AQP4, we used the technique of BN-PAGE (*23*−*25*), combined with immunoblotting. Conventional native gels were not successful (data not shown). The use of BN-PAGE requires non-ionic or zwitterionic detergents. We have previously screened a large series of detergents for their ability to solubilize AQP4 (*22*). For BN-PAGE, DDM at a detergent/protein ratio (w/w) of 2.2 turned out to give the optimal resolution (see Figure 1A). Identical results were obtained with DDM detergent/protein ratios up to 8, and also

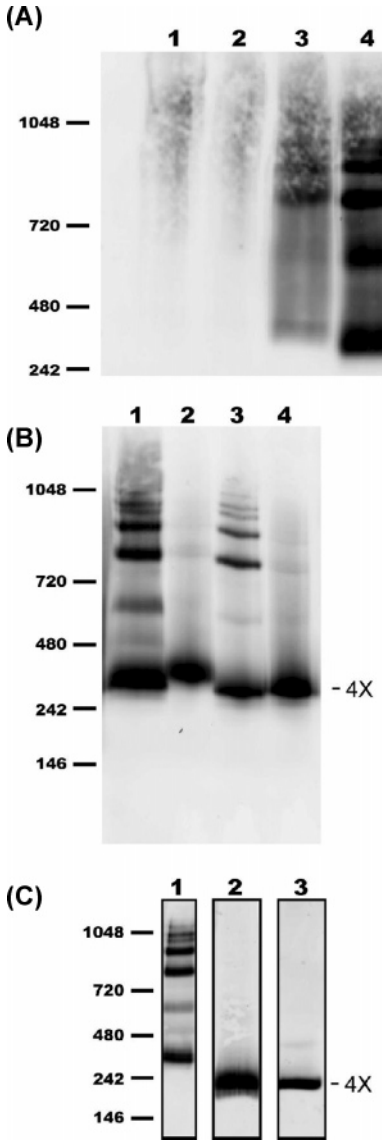

FIGURE 1: BN-PAGE analysis of AQP4 isoforms: (A) optimization detergent/protein ratio (w/w). Lanes 1, 2, 3, and 4 are ratios 0.6, 0.75, 1.1, and 2.2, respectively. (B) Comparison of rat brain AQP4 with transfected isoforms. Lane 1 is rat brain. Lanes 2, 3, and 4 are HeLa cells transfected with AQP4e, AQP4-M23, and AQP4-M1 cDNA, respectively. The putative tetramer is indicated as "4X", to the right. (C) BN-PAGE analysis of AQP1 and AQP9 show tetramer (4X, indicated to the right), but no higher-order structures (lanes 2 and 3, respectively), compared with AQP4 rat brain control (lane 1). Molecular weight marker indicated to the left (in kDa).

with a structurally unrelated zwitterionic detergent (data not shown).

BN-PAGE Visualizes Higher-Order Organization of AQP4 Isoforms. BN-PAGE immunoblots consistently showed a main band between the 242 kDa and 480 kDa markers (see Figure 1B), whereas a protein-only tetramer of AQP4 a priori would be observed at ~130 kDa. This discrepancy can, to some degree, be explained by the fact that the size of membrane proteins usually is overestimated by a factor of 1.8 ± 10% by BN-PAGE, because of the increased binding of Coomassie G-250, relative to the water-soluble marker proteins (described in detail in (*26*)). The AQP4 tetramer should run at 240 ± 24 kDa, which is in the lower range of what we observed. Thus, we interpret the main band as reflecting the AQP4 tetramer.

A series of higher bands, which is indicative of higher-order structures such as square arrays, appear above the tetramer, up to an apparent molecular weight of ~1000 kDa (see Figure 1B, lane 1). More bands were resolved in the BN-PAGE gel and can be observed in 2D-gel experiments (see discussion below), but a bias toward smaller complexes in the blotting of BN-PAGE gels precludes direct visualization of larger complexes.

The presence of six major bands between the tetramer band and ~1000 kDa (Figure 1B, lane 1) is consistent with aggregates of tetramers complexed with multiples of dimers of AQP4. A strong dimerization tendency of AQP4, even in denaturing SDS-PAGE gels, has been noted earlier (*27*). Head-to-head pairs of AQP0 tetramers have been demonstrated, using size exclusion chromatography for AQP0 (*28*).

The M23 and M1 monomers of AQP4 have molecular weights of 32.2 and 34.5 kDa, respectively. We observe seven major bands below ~1000 kDa. Theoretically, these bands might represent 4X, 6X, 8X, 10X, 12X, 14X, and 16X aggregates of monomers. The corresponding expected molecular weights would then be 238, 356, 475, 594, 713, 832, and 950 kDa, assuming an average monomer size of 33 kDa, and correcting with 1.8-fold dye binding (*26*). As a first approximation, assuming some variability in the molecular weight markers, and despite the slightly larger-than-expected size of the tetramer band (4X), this model of a square array tetramer core, with dimer additions, fits well with the observed BN-PAGE data.

Lysates from HeLa cells transfected with AQP4 isoforms M1, and a recently isolated new cDNA isoform called AQP4e (*29*), show only weak signs of higher-order structures, although they form strong tetramer bands (see Figure 1B, lane 4 and lane 2, respectively).

On the other hand, the transfected AQP4 isoform M23 is clearly able to form higher-order structures, with sizes matching those of rat brain lysate (see Figure 1B, lane 3). This is consistent with the reported ability of M23 to efficiently form square arrays in transfected cells (*12*, *19*), and with the failure of M1 to do so (*5*, *12*). Thus, the higher-order bands probably correspond to square arrays.

To provide additional support for the idea that the main band actually represents the tetramer, we probed blots with an AQP1 antibody, because it is firmly established that this aquaporin is organized as a tetramer (*30*, *31*). We expected the protein-only heterotetramer of AQP1 (monomers of 28 and 30 kDa, respectively) to be ~116 kDa. Correcting for 1.8-fold dye binding, we would expect AQP1 to run at 209 ± 21 kDa. The main AQP1 band appeared at 200 − 250 kDa (see Figure 1C, lane 2), which is consistent with AQP1 being a tetramer. Similarly, Aquaporin-9 (AQP9), which is a liver aquaporin, also shows only a tetramer band, and at an apparent molecular weight, is consistent with its monomer size (see Figure 1C, lane 3). Importantly, no higher-order bands for AQP1 and AQP9 were observed, which supports the aforementioned conclusion that the main AQP4 band is an AQP4 tetramer, and the higher-order AQP4 complexes correspond to square arrays.

Comparisons with Mouse Brain and Rat Nasal Mucosa. Comparing square arrays in rat brain with square arrays in mouse brain, it can be observed that the higher-order bands have approximately the same apparent size, even if the mouse signal is weaker and has less higher-order resolution (see

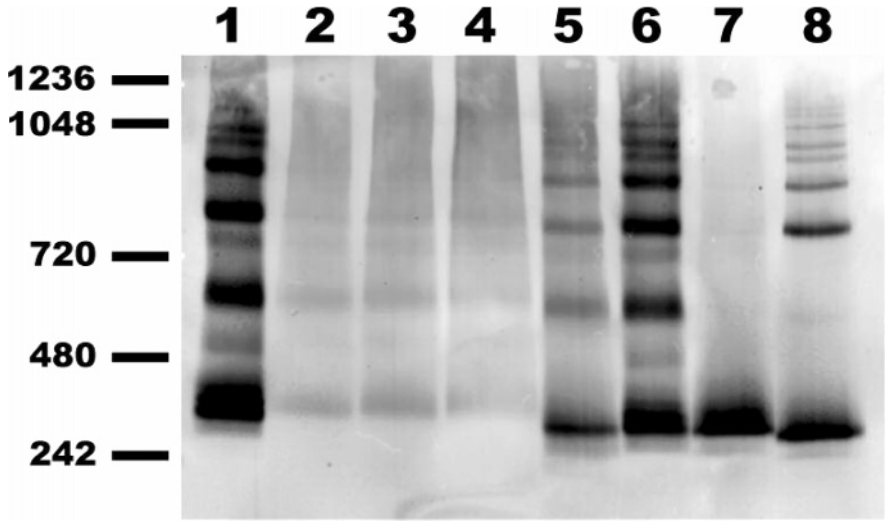

FIGURE 2: BN-PAGE comparison of square arrays in rat brain (lanes 1 and 6) with mouse brain (lanes 2, 3, and 4, with 40, 60, and 80 μg of total protein, respectively), and with nasal mucosa (lane 5, 20 μg of total protein). Lanes 7 and 8 are HeLa cells transfected with M1 or M23, respectively.

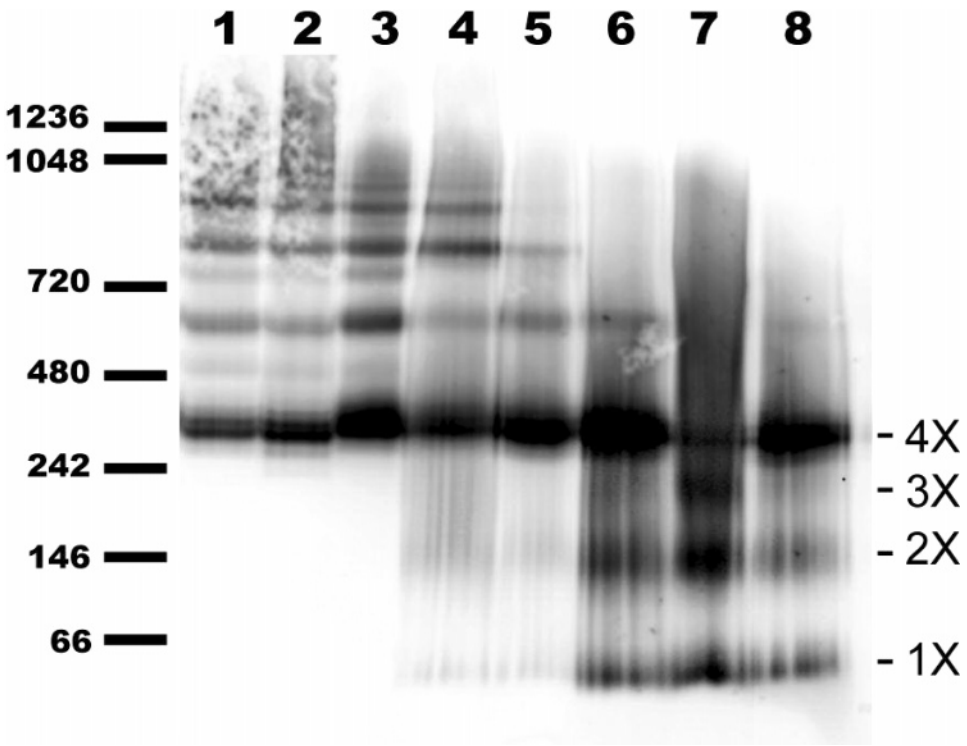

FIGURE 3: BN-PAGE analysis of rat brain AQP4 purification intermediates. Lane 1 is rat brain crude membranes, lane 2 is sucrose gradient purified plasma membranes, lane 3 is the alkaline membrane stripping fraction, lane 4 is detergent-solubilized membranes, and lane 5 is the ammonium sulfate precipitation fraction. Lanes 6−8 are different chromatographic elution fractions. The tetramer (4X), as well as the putative trimer (3X), dimer (2X), and monomer (1X), are indicated to the right.

Figure 2, lanes 1−4). It seems that AQP4 in the rat nasal mucosa (*32*, *33*), where AQP4 is expressed mainly in the respiratory epithelium and in Bowman gland cells in the olfactory epithelium (*34*), also has the same higher-order bands (see Figure 2, lane 5). However, the first minor intermediate band above the tetramer seems to be missing in the nasal mucosa (see Figure 2; compare lane 5 with lane 6). Whether this difference reflects a different function or a different composition of square arrays in the olfactory mucosa is presently unknown.

Square Arrays Are Stable during Biochemical Purification. Running various purification intermediates on BN-PAGE showed that the square arrays tolerate several enrichment, solubilization, and precipitation steps (see Figure 3, lanes 1−5). However, when subjected to chromatography, the higher-order structures are gradually lost, while three lower bands appear, most likely monomers, dimers, and trimers (see Figure 3, lanes 6−8). The stability of the square array pattern over several biochemical purification steps further supports the conclusion that the BN-PAGE observations reflect the diversity of square arrays in vivo.

Analysis of Square Array Monomer Composition by 2D Gels. On conventional 1D denaturing SDS-PAGE gels, a faint third AQP4 band, called Mz, is visible, in addition to the M23 and M1 bands (Figure 4A) (*35*). We have purified AQP4 from rat brain, and confirmed by mass spectrometry

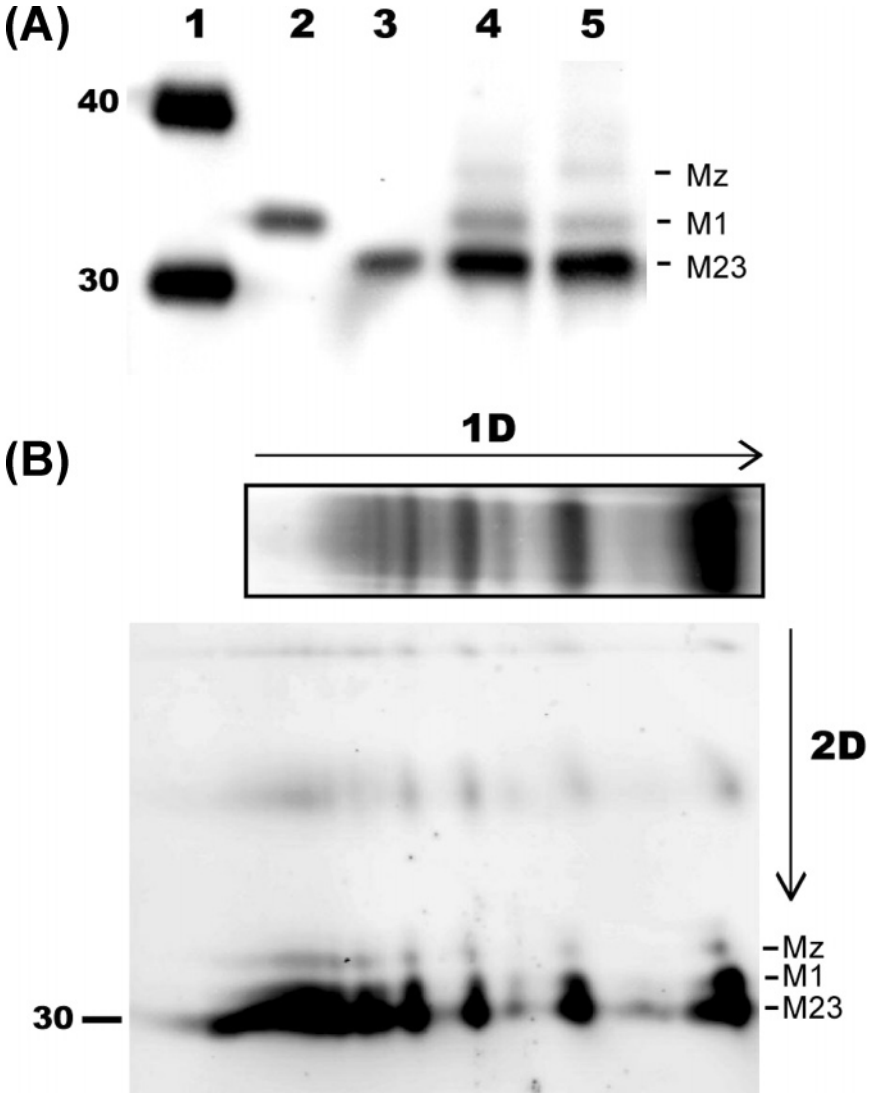

FIGURE 4: (A) SDS-PAGE analysis of lysates of HeLa cells transfected with M1 (lane 2) or M23 (lane 3), and lysates of rat hippocampus (lane 4) and rat cerebellum (lane 5). Size markers are shown in lane 1, with the molecular weight indicated on the left (in kDa), and the M1, M23, and Mz bands are indicated on the right. (B) 2D immunoblot of square arrays; rat brain membrane proteins were separated by BN-PAGE in the first dimension (upper panel, illustrative) and then again resolved by SDS-PAGE in the second dimension and immunoblotted (lower panel). Molecular weight marker at 30 kDa is shown to the left, and the M1, M23, and Mz bands are indicated on the right.

that the Mz band represents authentic AQP4 (Sorbo et al., unpublished).

To assess the composition of AQP4 isoforms in these higher-order structures, we coupled BN-PAGE to SDS-PAGE and immunoblotting, in a 2D gel setup. Each strong higher-order band in the first dimension (BN-PAGE) was resolved to Mz, M1, and M23 bands in the second dimension (SDS-PAGE) (see Figure 4B). The 2D analysis thus indicates that these three isoforms are all invariable components of square arrays.

Counting horizontally the bands visible after 2D SDS-PAGE gels, we estimate that at least 13 bands are visible within the resolution limit (see Figure 4B). Whether this limit reflects the upper size of square arrays in vivo is presently unknown, because we cannot exclude the possibility that there might also be additional, even higher-molecular-weight, structures that could not be identified using the present experimental approach.

CONCLUSION

The higher-order structures of aquaporin-4 (AQP4), which stands out as square arrays in freeze-fracture preparations, have attracted considerable attention (*1*−*5*, *10*−*12*, *19*−*21*). Here, we have established a new approach for analysis of square arrays, based on the use of Blue-Native PAGE (BN-PAGE) (*23*−*25*).

BN-PAGE analysis of rat brain membranes shows AQP4 complexes of high molecular weight that, in all likelihood, correspond to square arrays. This conclusion is supported by comparison with aquaporin-1 (AQP1) and aquaporin-9 (AQP9), which are known to form tetramers but no square arrays. Furthermore, transfection with AQP4 M1, and the recently isolated AQP4e isoform (*29*), gives bands that are indicative of tetramer formation, with little or no sign of higher bands. On the other hand, the transfected M23 isoform does show clear higher-order structures. This is consistent with detection of square arrays in CHO cells transfected with AQP4 M23, but not in cells transfected with M1 (*5*, *20*).

Our data imply a dominant role for AQP4 M23 in square array formation.

We have shown that AQP4 square arrays—in particular, the tetramer—are stable during initial purification steps, while, during chromatographic steps, a gradual breakdown is observed. This behavior is most likely due to delipidation during column washing: this is a procedure that is known to provoke denaturation and inactivation (*36*). The breakdown of the square arrays to probable trimers, dimers, and monomers lends further support to the notion that we are observing AQP4 tetramers with BN-PAGE methodology, and that this methodology can be used to analyze square arrays.

The higher-order bands observed on BN-PAGE are consistent with tetramers aggregating with multiples of dimers. The observation that the AQP4 higher-order structures are composed of multiples of dimers is consistent with the strong dimerization tendency of AQP4 (*27*). Interestingly, our consistent observation of a rather too-high size estimate of the AQP4 tetramer band, and the gradual loss of higher-order structures under biochemical purification, might indicate that an unknown component is present along with the AQP4 tetramers. This would be consistent with the observed presence of material between the monomers in freeze-fracture studies (*5*).

Our finding, in 2D gel immunoblots, that M1 and the third isoform Mz are invariable components of the higher-order structures provides the first evidence that M1 and Mz are constituents of native square arrays. A ~10:1 ratio between the AQP4 M23 and M1 isoforms has been reported (*35*) and recently validated in a series of brain tissues (Sorbo et al., unpublished). When combining this ratio with the presence of the even-fainter Mz band, stoichiometric considerations imply a heterogeneous population of AQP4 multimers in the brain. For example, a universal tetramer that consisted of M23, M1, and Mz would have resulted in a 2:1:1 ratio. Thus, it seems likely that a spectrum of AQP4 complexes exists in vivo (*5*), which indicates a similar complexity, in terms of function.

ACKNOWLEDGMENT

We thank Søren Nielsen for the M1 and M23 plasmids.

REFERENCES

1. Dermietzel, R. (1973) Visualization by freeze-fracturing of regular structures in glial cell membranes, *Naturwissenschaften 60*, 208.
2. Wolburg, H. (1995) Orthogonal arrays of intramembranous particles: a review with special reference to astrocytes, *J. Hirnforsch. 36*, 239−258.
3. Rash, J. E., Staehelin, L. A., and Ellisman, M. H. (1974) Rectangular arrays of particles on freeze-cleaved plasma membranes are not gap junctions, *Exp. Cell Res. 86*, 187−190.
4. Landis, D. M., and Reese, T. S. (1974) Arrays of particles in freeze-fractured astrocytic membranes, *J. Cell Biol. 60*, 316−320.
5. Rash, J. E., Davidson, K. G., Yasumura, T., and Furman, C. S. (2004) Freeze-fracture and immunogold analysis of aquaporin-4 (AQP4) square arrays, with models of AQP4 lattice assembly, *Neuroscience 129*, 915−934.
6. Hiroaki, Y., Tani, K., Kamegawa, A., Gyobu, N., Nishikawa, K., Suzuki, H., Walz, T., Sasaki, S., Mitsuoka, K., Kimura, K., Mizoguchi, A., and Fujiyoshi, Y. (2006) Implications of the aquaporin-4 structure on array formation and cell adhesion, *J. Mol. Biol. 355*, 628−639.
7. Gonen, T., Cheng, Y., Sliz, P., Hiroaki, Y., Fujiyoshi, Y., Harrison, S. C., and Walz, T. (2005) Lipid-protein interactions in double-layered two-dimensional AQP0 crystals, *Nature 438*, 633−638.
8. Scheuring, S., Buzhynskyy, N., Jaroslawski, S., Goncalves, R. P., Hite, R. K., and Walz, T. (2007) Structural models of the supramolecular organization of AQP0 and connexons in junctional microdomains, *J. Struct. Biol. 160*, 385−394.
9. Buzhynskyy, N., Girmens, J. F., Faigle, W., and Scheuring, S. (2007) Human cataract lens membrane at subnanometer resolution, *J. Mol. Biol. 374*, 162−169.
10. Frigeri, A., Gropper, M. A., Umenishi, F., Kawashima, M., Brown, D., and Verkman, A. S. (1995) Localization of MIWC and GLIP water channel homologs in neuromuscular, epithelial and glandular tissues, *J. Cell Sci. 108 (Pt 9)*, 2993−3002.
11. Verbavatz, J. M., Ma, T., Gobin, R., and Verkman, A. S. (1997) Absence of orthogonal arrays in kidney, brain and muscle from transgenic knockout mice lacking water channel aquaporin-4, *J. Cell Sci. 110 (Pt 22)*, 2855−2860.
12. Rash, J. E., Yasumura, T., Hudson, C. S., Agre, P., and Nielsen, S. (1998) Direct immunogold labeling of aquaporin-4 in square arrays of astrocyte and ependymocyte plasma membranes in rat brain and spinal cord, *Proc. Natl. Acad. Sci., U.S.A. 95*, 11981−11986.
13. Wakayama, Y., Takahashi, J., Shibuya, S., Inoue, M., Kojima, H., Oniki, H., Arata, S., Hara, H., Jimi, T., Shioda, S., Sunada, Y., Ohi, H., and Shimizu, T. (2007) Generation of muscle aquaporin 4 overexpressing transgenic mouse: its characterization at RNA and protein levels including freeze-fracture study, *Micron 38*, 257−267.
14. King, L. S., Kozono, D., and Agre, P. (2004) From structure to disease: the evolving tale of aquaporin biology, *Nat. Rev. Mol. Cell Biol. 5*, 687−698.
15. Nielsen, S., Nagelhus, E. A., Amiry-Moghaddam, M., Bourque, C., Agre, P., and Ottersen, O. P. (1997) Specialized membrane domains for water transport in glial cells: high-resolution immunogold cytochemistry of aquaporin-4 in rat brain, *J. Neurosci. 17*, 171−180.
16. Verkman, A. S., Binder, D. K., Bloch, O., Auguste, K., and Papadopoulos, M. C. (2006) Three distinct roles of aquaporin-4 in brain function revealed by knockout mice, *Biochim. Biophys. Acta 1758*, 1085−1093.
17. Amiry-Moghaddam, M., and Ottersen, O. P. (2003) The molecular basis of water transport in the brain, *Nat. Rev. Neurosci. 4*, 991−1001.
18. Manley, G. T., Fujimura, M., Ma, T., Noshita, N., Filiz, F., Bollen, A. W., Chan, P., and Verkman, A. S. (2000) Aquaporin-4 deletion in mice reduces brain edema after acute water intoxication and ischemic stroke, *Nat. Med. 6*, 159−163.
19. Yang, B., Brown, D., and Verkman, A. S. (1996) The mercurial insensitive water channel (AQP-4) forms orthogonal arrays in stably transfected Chinese hamster ovary cells, *J. Biol. Chem. 271*, 4577−4580.
20. Furman, C. S., Gorelick-Feldman, D. A., Davidson, K. G., Yasumura, T., Neely, J. D., Agre, P., and Rash, J. E. (2003) Aquaporin-4 square array assembly: opposing actions of M1 and M23 isoforms, *Proc. Natl. Acad. Sci., U.S.A. 100*, 13609−13614.
21. Silberstein, C., Bouley, R., Huang, Y., Fang, P., Pastor-Soler, N., Brown, D., and Van Hoek, A. N. (2004) Membrane organization and function of M1 and M23 isoforms of aquaporin-4 in epithelial cells, *Am. J. Physiol. Renal Physiol. 287*, F501−F511.
22. Sorbo, J. G., Moe, S. E., and Holen, T. (2007) Early upregulation in nasal epithelium and strong expression in olfactory bulb glomeruli suggest a role for Aquaporin-4 in olfaction, *FEBS Lett. 581*, 4884−4890.
23. Schagger, H., and von Jagow, G. (1991) Blue native electrophoresis for isolation of membrane protein complexes in enzymatically active form, *Anal. Biochem. 199*, 223−231.
24. Schagger, H., Cramer, W. A., and von Jagow, G. (1994) Analysis of molecular masses and oligomeric states of protein complexes by blue native electrophoresis and isolation of membrane protein complexes by two-dimensional native electrophoresis, *Anal. Biochem. 217*, 220−230.
25. Wittig, I., Braun, H.-P., and Schägger, H. (2006) Blue Native PAGE, *Nat. Protoc. 1 (1)*, 418−428.
26. Heuberger, E. H., Veenhoff, L. M., Duurkens, R. H., Friesen, R. H., and Poolman, B. (2002) Oligomeric state of membrane transport proteins analyzed with blue native electrophoresis and analytical ultracentrifugation, *J. Mol. Biol. 317*, 591−600.
27. Lu, M., Lee, M. D., Smith, B. L., Jung, J. S., Agre, P., Verdijk, M. A., Merkx, G., Rijss, J. P., and Deen, P. M. (1996) The human

AQP4 gene: definition of the locus encoding two water channel polypeptides in brain, *Proc. Natl. Acad. Sci., U.S.A. 93*, 10908−10912.
28. Gonen, T., Cheng, Y., Kistler, J., and Walz, T. (2004) Aquaporin-0 membrane junctions form upon proteolytic cleavage, *J. Mol. Biol. 342*, 1337−1345.
29. Moe, S. E., Sorbo, J. G., Sogaard, R., Zeuthen, T., Ottersen, O. P., and Holen, T. (2007) New Isoforms of rat AQP4, *Genomics* (in press).
30. Smith, B. L., and Agre, P. (1991) Erythrocyte Mr 28,000 transmembrane protein exists as a multisubunit oligomer similar to channel proteins, *J. Biol. Chem. 266*, 6407−6415.
31. Verbavatz, J. M., Brown, D., Sabolic, I., Valenti, G., Ausiello, D. A., Van Hoek, A. N., Ma, T., and Verkman, A. S. (1993) Tetrameric assembly of CHIP28 water channels in liposomes and cell membranes: a freeze-fracture study, *J. Cell Biol. 123*, 605−618.
32. Rash, J. E., Davidson, K. G., Kamasawa, N., Yasumura, T., Kamasawa, M., Zhang, C., Michaels, R., Restrepo, D., Ottersen, O. P., Olson, C. O., and Nagy, J. I. (2005) Ultrastructural localization of connexins (Cx36, Cx43, Cx45), glutamate receptors and aquaporin-4 in rodent olfactory mucosa, olfactory nerve and olfactory bulb, *J. Neurocytol. 34*, 307−341.
33. King, L. S., Nielsen, S., and Agre, P. (1997) Aquaporins in complex tissues. I. Developmental patterns in respiratory and glandular tissues of rat, *Am. J. Physiol. 273*, C1541−C1548.
34. Ablimit, A., Matsuzaki, T., Tajika, Y., Aoki, T., Hagiwara, H., and Takata, K. (2006) Immunolocalization of water channel aquaporins in the nasal olfactory mucosa, *Arch. Histol. Cytol. 69*, 1−12.
35. Neely, J. D., Christensen, B. M., Nielsen, S., and Agre, P. (1999) Heterotetrameric composition of aquaporin-4 water channels, *Biochemistry 38*, 11156−11163.
36. Hunte, C., von, J. G., and Schagger, H. (1994) *Membrane Protein Purification and Crystallization: A Practical Guide*, Academic Press, New York.

BI702146K